Received: 2 November 2022 | Revised: 1 December 2022 | Accepted: 10 December 2022

DOI: 10.1111/ter.12641

RESEARCH ARTICLE

Terra Nova WILEY

Large landslide of the hyperarid Central Western Andes triggered during a humid period of the Late Pleistocene (ca. 19°S; northern Chile)

Swann Zerathe | Laurence Audin | Xavier Robert | Stéphane Schwartz | Julien Carcaillet

ISTerre, IRD, CNRS, Univ. Grenoble Alpes, USMB, Grenoble, France

Correspondence
Swann Zerathe, ISTerre, IRD, CNRS, Univ. Grenoble Alpes, USMB, 38000, Grenoble, France.
Email: swann.zerathe@ird.fr

Abstract

The western flank of the Central Andes offers a unique geomorphological record of large paleolandslides that are well preserved on long time-scales (i.e. ≥Pleistocene) due to the long-lasting aridity of this region. However, the lack of chronological constraints on those landslides limits our understanding of the respective role of tectonics and climate on their triggering. Here, we report new ^{10}Be surface exposure dating obtained on one of those giant slope-failures: the Limaxina landslide (northern Chile, 19°S). Five tightly grouped exposure-ages (one outlier discarded) point to a single landslide failure at 80 ± 4 ka. This timing being consistent with others local records of a wet episode in the Atacama Desert, it suggests a primary role of climate-forcing on landslide activity in this region, calling to further slope failures dating in the arid Central western Andes to explore landscapes responses to Quaternary climate oscillations and extreme events.

1 | INTRODUCTION

Along the Central Western Andes of southern Peru and northern Chile, hundreds of giant paleo-landslides involving volumes up to several cubic kilometres of rocks debris were recently inventoried and geomorphologically characterized (Figure 1; Delgado et al., 2022). The conditions of trigger of these slope failures, that could be related to past climate changes (e.g. Margirier et al., 2015) and/or strong seismo-tectonic forcings (e.g. Crosta et al., 2017), remain an uncertain and opened debate within the scientific community (e.g. Delgado et al., 2020, 2022; Moreiras & Sepúlveda, 2015). Indeed, the presence of such deep and giant slope instabilities, implying strong landscape perturbations, is paradoxical given that hyperarid conditions prevails in this region—the so-called Atacama Desert—since at least 10–12 Ma (e.g. Dunai et al., 2005; Rech et al., 2019). On the other hand, those extremely dry condition, preserving the landscapes from erosion, offers an interesting opportunity to study the evolution of landslides on long time-scales (i.e. Quaternary) that are generally not available in temperate regions where the geological records of landslides in high mountains are usually erased by stronger fluvial and glacial erosion, and where landslide studies are mainly restricted to the Holocene (e.g. Pánek & Klimeš, 2016). However, the great majority of the large landslides identified along the Central Western Andes remains undated (Delgado et al., 2022), thus hampering our ability to evaluate their frequency of occurrence and to decipher their possible relations with seismic or climatic destabilizing factors.

In order to contribute to current works to solve those questions, we provide a geomorphological and geochronological analysis of the Limaxina large landslide located at ca. 19.77° S–69.18° W along the

Western Cordillera of northern Chile. We applied in-situ produced ^{10}Be exposure dating on boulders of the landslide debris. The comparison of the Limaxina landslide age with regional paleo-climate records indicates a dominant climatic triggering during a major Late Pleistocene wet event.

2 | SETTINGS: TECTONIC, CLIMATE AND GIANT LANDSLIDES OF THE CENTRAL WESTERN ANDES

The study area locates along the western flank of the Central Andes of northern Chile at ca. 19–20°S (Figure 1a). The region is divided into four main morphotectonic provinces: the Coastal Cordillera, the Longitudinal Basin, the Western Cordillera and the Altiplano (Figure 1b). The Andean orogen results from more than 50 Ma of plates convergence, involving the subduction of the Nazca plate below the South American plate, producing long-term crustal thickening and volcanism, as well as strongly coupled tectonic and climate processes acting on the relief evolution (see the extensive review of Armijo et al., 2015). The entire region is tectonically active: mega-earthquakes of Mw>8 frequently occur (ca. every 200 years; e.g. Chlieh et al., 2011) along the subduction (e.g. Metois et al., 2016); uplift is ongoing in the Coastal and the Western Cordillera as documented by raised marine terraces (e.g. Binnie et al., 2016) and incised/abandoned paleo fluvial surfaces (e.g. Evenstar et al., 2017, 2020), respectively; numerous neotectonics crustal faults (Figure 1b) capable of Mw6-7 earthquakes dissect the Coastal Cordillera (e.g. Cortés-Aranda et al., 2021; Maldonado et al., 2021); west-verging, buried, main thrusts located at the front of the Western Cordillera (Figure 1c,e,g; Armijo et al., 2015; Martínez et al., 2021) can have also a strong seismic potential (e.g. Herrera et al., 2021).

A specificity of the Central Western Andes is its hyperarid climate prevailing since at least the Miocene (Rech et al., 2019) and making the Atacama Desert one of the driest and oldest desert on Earth (Hartley et al., 2005) which enable exceptionally long landscape preservation due to slow, long-term erosion (Dunai et al., 2005). These dry conditions have been related to several factors, including the mid-latitude of this region under the influence of the subtropical high-pressure belt, the cold upwelling water of the Humboldt Current, cooling air and retaining moisture at the surface, and the rain shadow effect of the Andean relief blocking any moisture transfer from the Amazonian humidity (Houston & Hartley, 2003). On the other hand, short (hours to few days) intense storms with strong run-off (e.g. Bozkurt et al., 2016) can occur in response to El Niño-La Niña oscillations (ENSO). Geomorphological evidences and paleoclimatic proxies have also reported the occurrence of possibly more persistent humid conditions during previous Pleistocene interglacial periods as marked by paleolake shorelines (Ritter et al., 2018), alluvial fans and sediment aggradation (e.g. Ritter et al., 2019), paleo-wetlands formation (e.g. Roperch et al., 2017).

In this context, another particularity of the region is that giant paleo landslides are ubiquitous (Figure 1). Delgado et al. (2022) indicate that their formation was favoured by coupled conditioning factors including lithology and strong local relief generated by the incision of deep canyons through the Western Cordillera. In particular, spatial clustering was highlighted by the presence of dozens of large landslides concentrated within few kilometres such as all-around the Limaxina landslide (Figures 1c and 2a). However, the timing of most of these landslides being largely unknown, discussion about the respective roles of climate or tectonic on their triggering remain speculative up to now and required additional data.

Statement of significance

The arid area of Central Andes holds, at the Earth scale, one of the highest concentrations of large preserved paleo-landslides. Their presence has been related to the strong relief produced along the tectonically growing Andes and their uncommonly high spatial density is likely due to the long-term preservation of landscapes in the extremely dry conditions of the Atacama Desert. However, unsolved ambiguity remains about the respective roles of climate or earthquake on their triggering. Here we document a temporal correlation between a large landslide dated at 80±4 ka along the Western Cordillera of northern Chile and a humid climate period identified in a recently published paleoenvironmental records from the near Atacama core. Adding a compilation of previously dated landslides also shows synchronous triggering with other regional Late Pleistocene humid phases. This study suggests that past climate changes, owing to more humid conditions, were the primary factors controlling giant landslide occurrence along the arid western flank of the Central Andes.

3 | GEOMORPHOLOGY OF THE LIMAXINA LARGE LANDSLIDE

The Limaxina landslide locates in the upper part of the Quebrada Tarapaca (Figure 2a), where it eroded a paleo fluvial surface abandoned since the Late Miocene (Evenstar et al., 2017). The slope failure affected a Neogene volcanic series composed of andesite and ignimbrites interbedded with rhyolites that are overlying a thick Cretaceous sedimentary sequence of shales, sandstones and conglomerates (Figure 2a). This mechanical context, with hard rock overlying soft rock, may have been an important predisposing factor for the Limaxina landslide and the numerous other slope instabilities in this area (Figure 2a). The Limaxina landslide covers an area of ca. 16 km^2 and its failure left impressive geomorphological glimpses on the landscape (Figure 2). A headscarp of ~5 km long, 200–400 m high, bounds the paleo-landslide to the north (Figure 2b,c). Morphologies such as transversal and longitudinal ridges are observed at the landslide surface suggesting compressive and shear

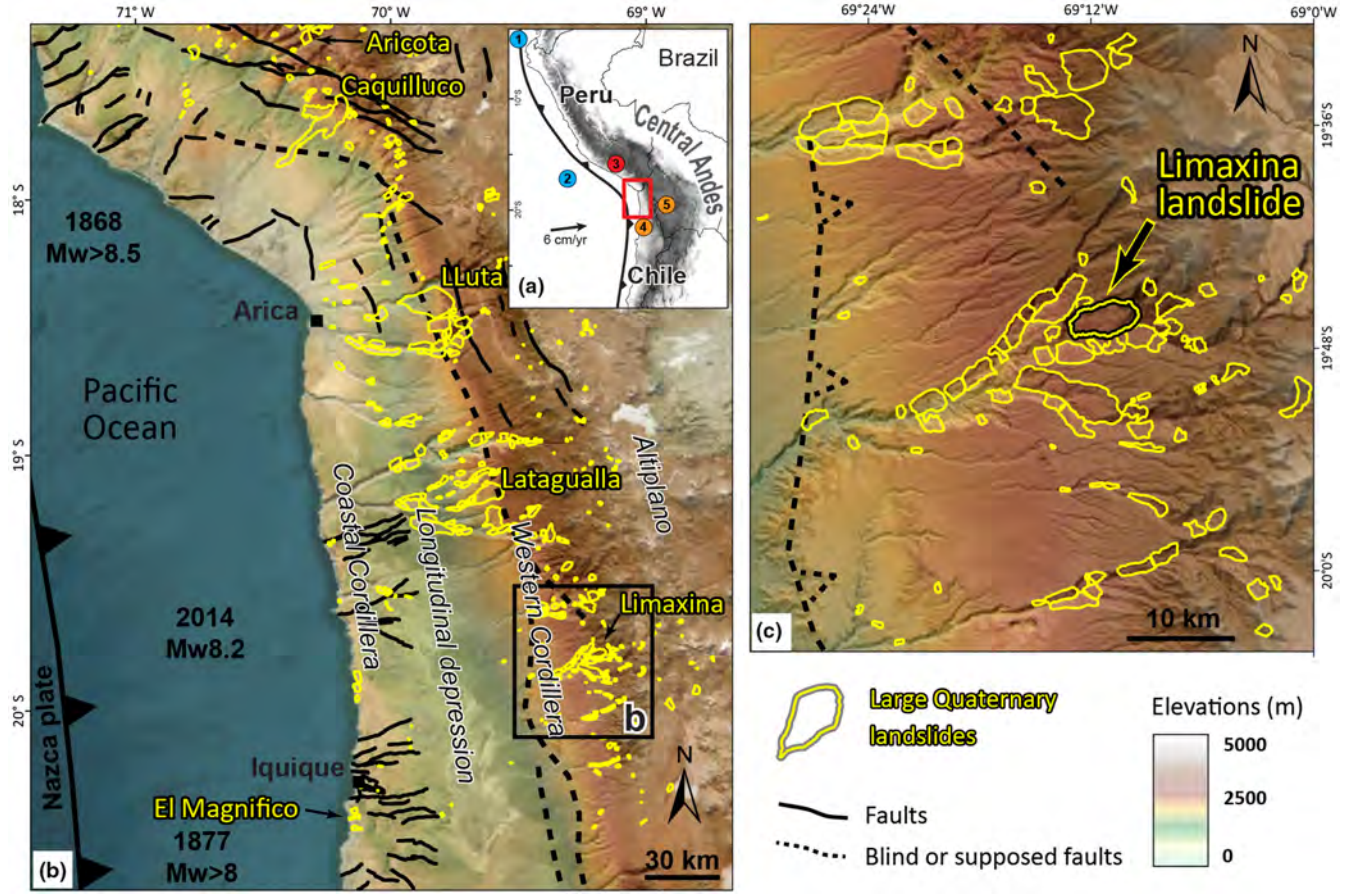

FIGURE 1 (a) Study area location along the Central Western Andes. The numbered items correspond to previous studies cited here after. 1: Marine record ODP 1239 (Rincón-Martínez et al., 2010); 2: Marine record TG7 (Calvo et al., 2001); 3: Chuquibamba landslide (Margirier et al., 2015); 4: Paleoclimate record of the Atacama Desert (Ritter et al. (2019); 5: Paleoclimate record of Altiplano lakes and Salars (Placzek et al., 2006, 2013). (b) ASTER DEM of the Central Western Andes of southern Peru and northern Chile showing the seismo-tectonic context and the distribution of the large paleo-landslides as inventoried by Delgado et al. (2022). Recent and historic mega-earthquakes of subduction are reported from Villegas-Lanza et al. (2016) and Metois et al. (2016), and crustal faults are from Armijo et al. (2015) and Maldonado et al. (2021). Some of the largest landslides are pointed: Aricota (Delgado et al., 2020); Caquilluco (Crosta et al., 2014); Lluta (Strasser & Schlunegger, 2005); Lataguallla (Pinto et al., 2008), El Magnifico (Crosta et al., 2017) and Limaxina (this study). (c) Close-up on the Western cordillera at 19–20°S where the Limaxina landslide locates

deformation, respectively (Figure 3a). On the other hand, the landslide surface morphology appears rather as a unique slided mass, over which we did not observe any major contact, nor evidence of superimposed debris deposits, favouring the interpretation of the occurrence of a single failure event. No sign of present-day activity of the landslide mass was observed during our fieldtrip. At some places, incisions of gullies through the landslide body highlight debris thickness >30 m (Figure 3b). At surface, we noted boulder's accumulation of pluri-metric size (Figure 3). At the landslide toe, we observed the contact between the slided mass and the underlying substratum (Figure 3b,c). This contact is marked by a sharp and thin (only few centimetres thick) shearing surface that is accompanied by plastic deformations of the underlying shales (Figure 3d). This suggests a significant water content in the landslide debris and in the sedimentary substratum. Upstream to the landslide body, the valley of Tarapaca is filled by lacustrine deposits which indicates that the landslide temporarily dammed the valley (Figure 3e). A paleo-shoreline stands at 1750 m a.s.l. (Figure 3e). Compiling these observations, we evaluated a landslide deposit thickness varying between 30 and 100 m (Figure 2c) and a mean volume of debris of ca. 1 km^3.

4 | ^{10}Be COSMOGENIC NUCLIDE DATING

Six boulders located in the middle of the Limaxina landslide body (Figure 2b) were sampled for ^{10}Be surface exposure dating. We selected some the largest boulders (height >1 m), avoiding any significant trace of erosion, nor desquamation (Figure 4). The rhyolite lithology allowed the use of the classic ^{10}Be-quartz pair. Sample preparation and ^{10}Be chemical extraction were performed at the GTC Platform laboratory, ISTerre (Grenoble, France), following the routinely used ^{10}Be extraction protocol of Corbett et al. (2016) (also see protocol details in Delgado et al., 2020).

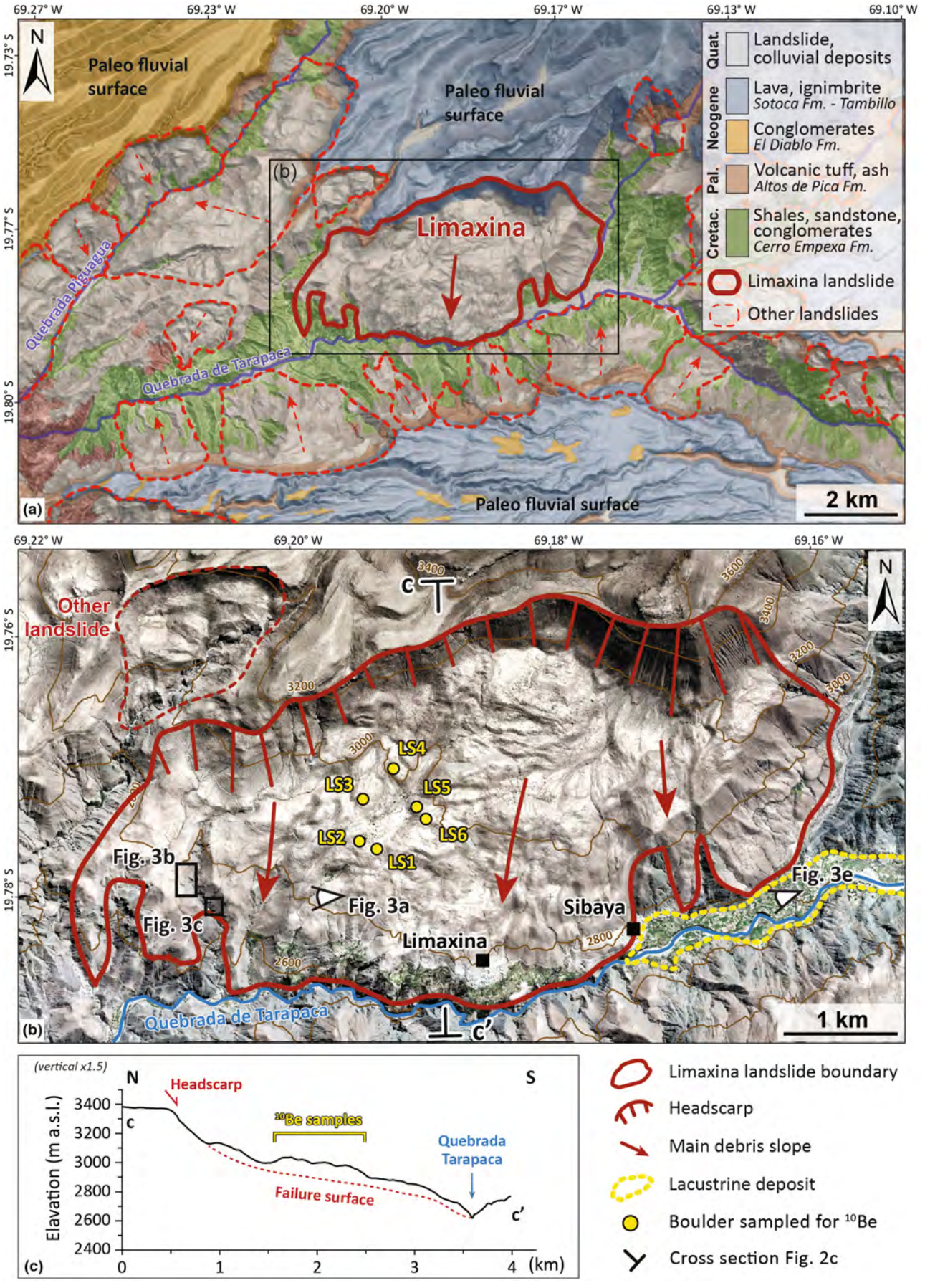

FIGURE 2 (a) Geological map around the Limaxina landslide (simplified from Morandé et al., 2015). The paleo fluvial surface (Late Miocene age) is reported from Evenstar et al. (2017). (b) Geomorphological map (Google earth view) of the Limaxina landslide showing the main gravitational features and the location of boulders sampled for ^{10}Be dating. The red arrows show the movement direction. (c) Interpreted cross-section of the landslide (see location on b)

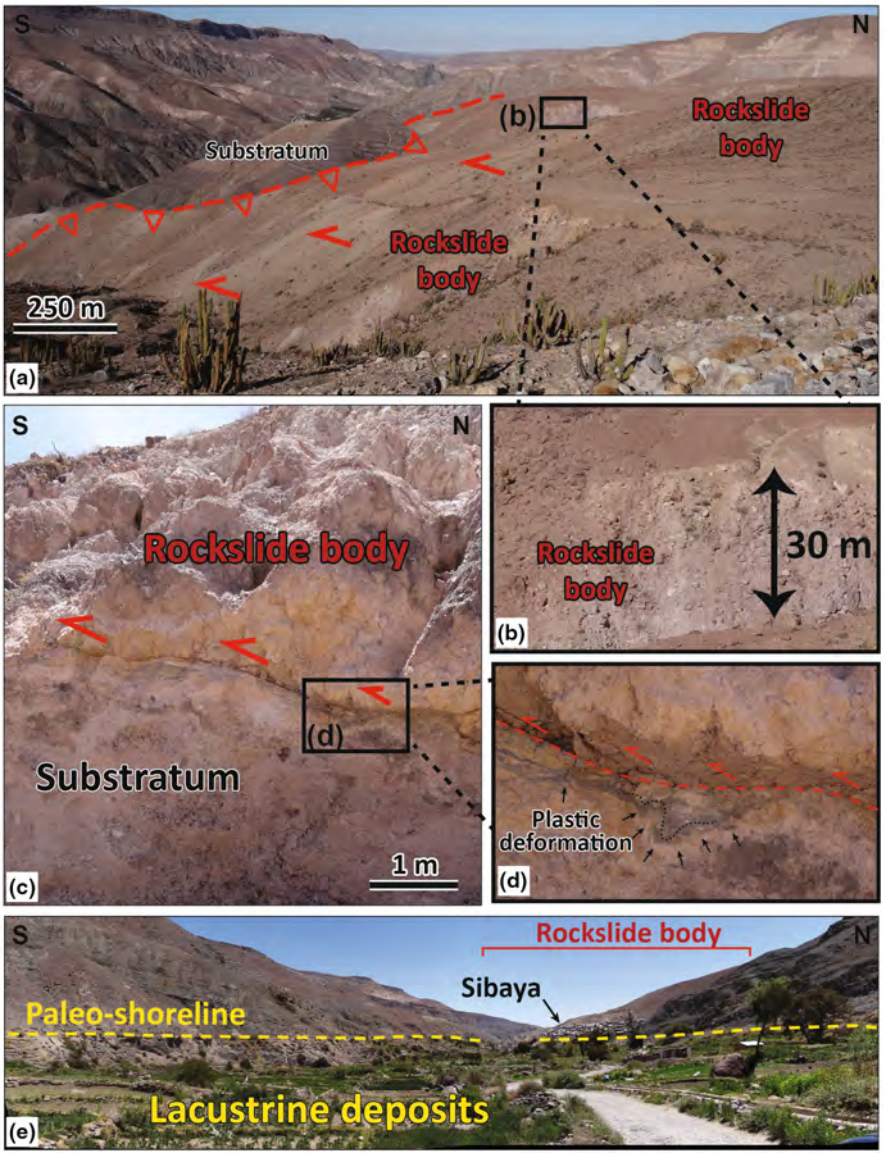

FIGURE 3 Panoramic and close-up views of the main gravitational features associated to the Limaxina landslide (see location of each photo on Figure 2a). (a) Panoramic view toward the west from the middle of the landslide body showing how landslide debris overlapped the substratum characterized by intercalating shales and sandstone. The red arrows show the movement direction. (b) Fluvial re-incision through the landslide body showing a 30 m thick accumulation of debris and crushed material. (c) and (d) shearing contact (red arrows) between the substratum and the landslide body. Striaes confirming the displacement direction toward downstream are observed along the contact. (d) Zoom on substratum, below the failure surface, affected by plastic deformations (pointed by the black arrows) suggesting the presence of water in the medium. (e) Panoramic view looking downward from the lacustrine deposit. A paleo-lake shoreline stands at ~1750 m a.s.l.

The ^{10}Be/^{9}Be measurements were performed at the French national accelerator ASTER, located at CEREGE in Aix-en-Provence (Arnold et al., 2013). The ^{10}Be/^{9}Be ratios were calibrated against the internal standard STD-11, using an assigned ^{10}Be/^{9}Be ratio of $(1.191 \pm 0.013) \times 10^{-11}$ (Braucher et al., 2015). Uncertainties in the ^{10}Be concentrations (reported as 1σ) are calculated according to the standard error propagation method using the quadratic sum of the relative errors and include a conservative 0.5% external uncertainty in the machine (Arnold et al., 2010), a 1.09% uncertainty in the certified standard ratio, a 1σ uncertainty associated with the mean of the standard ratio measurements over measurement cycles, a 1σ statistical error in the counted events, and the uncertainty associated with the chemical and analytical correction of the blank. Exposure ages were computed using the CREP online calculator (Martin et al., 2017), applying the World-wide mean, and time-dependent, ^{10}Be spallation production rate of 4.06 ± 0.23 at.gr^{-1}.year^{-1} (Borchers et al., 2016) scaled to the geographic and altitudinal location of each boulder and parametrized using the LSD scaling scheme (Lifton et al., 2014), the Lifton VDM 2016 geomagnetic database, and the ERA40 atmosphere model (see references in Martin et al., 2017). A mean denudation rate of 0.2 mm. ka^{-1} was applied, as constrained by Placzek et al. (2010) at ~24° S for boulders of the Atacama desert. Using a zero-denudation leads to a difference <2% in the final result. Raw data formatted for the CREp template are provided in Material S3 to allow for recalculation using alternative parametrization.

FIGURE 4 Pictures of the sampled boulders. See location on Figure 2a and related data in Table 1

We obtained five exposure ages that are ranged from 73.8 ± 5.2 to 86.0 ± 5.3 ka (LS1, LS2, LS4, LS5 and LS6) and one exposure age of 272.0 ± 16.1 ka (LS3) (Table 1). A graphical analysis of the age distribution through a probability density plot, as well as a chi-squared test (Figure 5), both show that the five ages ranged between from ~74 to ~86 ka are tightly grouped, overlaping within their uncertainties and pointing to weighted-mean age of 80 ± 4 (Figure 5). As the sample LS3 is significantly older (Figure 5), it may be considered as an outlier. It might be related to an older previous slope failure on the Limaxina site, or, more likely, to an inherited component of ^{10}Be. In such arid setting, the production and accumulation of cosmogenic nuclide can be significant even at great depth (i.e. up to ~20 m depth; e.g. Braucher et al., 2013; Delgado et al., 2020; Hilger et al., 2019) because surface denudation rates are very low. In summary, we retain a weighted-mean age of 80 ± 4 ka (1σ weighted standard deviation) for the Limaxina landslide failure, pointing to a single and major slope failure event, which is consistent with the geomorphological observations.

5 | DISCUSSION: TRIGGERING CONDITIONS OF THE LIMAXINA LANDSLIDE

Due to the long-term convergence between the Nazca and South American plates, the Central Andes is a geodynamically particularly active region. In this context, a seismo-tectonic forcing has been often a preferred interpretation to explain the triggering of paleolandslides

TABLE 1 ^{10}Be data

Label	Latitude (°S)	Longitude (°W)	Elevation (m.a.s.l.)	Thick. (cm)	Sheild. Factor	Mass (g)	^{9}Be (10^{19} at)	^{10}Be counts	^{10}Be/^{9}Be (10^{-13})	^{10}Be[a] (10^{6} at.g^{-1})	Age[b] (ka)
LS 1	19.77633	69.19332	2910	1.0	0.98	4.803	3.53	2280	2.06 ± 0.06	1.51 ± 0.04	79.9 ± 5.0 (2.3)
LS 2	19.77574	69.19466	2910	1.0	0.98	4.836	3.51	2038	2.15 ± 0.06	1.55 ± 0.04	82.5 ± 5.2 (2.3)
LS 3	19.77249	69.19439	2947	1.0	0.98	4.676	3.58	1278	6.85 ± 0.21	5.24 ± 0.16	272.0 ± 16.1 (7.5)
LS 4	19.77015	69.19205	2987	0.5	0.98	4.286	3.52	1225	2.08 ± 0.06	1.70 ± 0.05	86.0 ± 5.3 (2.6)
LS 5	19.77310	69.19026	2960	2.0	0.98	4.666	3.52	1294	2.04 ± 0.06	1.53 ± 0.05	79.5 ± 5.1 (2.5)
LS 6	19.77402	69.18955	2959	3.0	0.98	4.486	3.52	1117	1.81 ± 0.07	1.42 ± 0.05	73.8 ± 5.2 (2.9)

[a]Uncertainties are 1σ external uncertainties (including all the uncertainties, see Section 4 for details), internal uncertainties (Production rate uncertainty not considered) are provided between brackets.
[b]Analytical uncertainties are 1σ and include the counting statistics, the machine stability (~0.5%) and the blank correction based on a ^{10}Be/^{9}Be blank ratio of $(8.0 \pm 1.7) \times 10^{-16}$ for those samples.

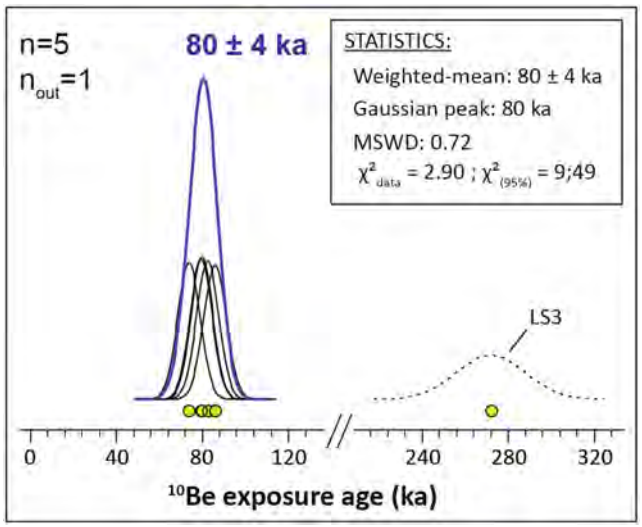

FIGURE 5 Probability density plot of exposure ages obtained from boulders of the Limaxina landslide (plot built using the DensityPlotter software from P. Vermeesch, London geochronology Centre). Thin black curves are individual gaussian of the exposure ages while the thick blue curve is the summed probability density function of the population. Dashed curve corresponds to the exposure age of sample LS3 that is considered as an outlier (see text for explanation)

(e.g. Crosta et al., 2014, 2015; Mather et al., 2014; McPhillips et al., 2014; Pinto et al., 2008; Strasser & Schlunegger, 2005). On the eastern Precordillera, Junquera-Torrado et al. (2021) tried to link paleo-landslides to their potential seismic source along crustal faults. Similarly, a seismic triggering can be a possible option for the Limaxina landslide because it stands just along a major blind thrust fault bounding the Western Cordillera (Figure 1c; Armijo et al., 2015). However, the paleo-seismicity of this fault system is largely unknown and such link would remain thus speculative. Along the coastal cordillera of northern Chile, Crosta et al. (2017) proposed a seismic origin, linked to the mega-earthquakes of subduction, for the triggering of the El Magnifico rock-avalanche paleo cluster. However, after the recent mega-earthquake of Iquique (Mw8.2, 2014) only small rockfalls were observed. This strong earthquake did not trigger, nor reactivated, any large slope failure (Candia et al., 2017). Post-seismic observations after each of the recent and historical strong subduction earthquakes that affected southern Peru and northern Chile point out the absence of large landslide triggering (>10 km^2; e.g. Keefer & Moseley, 2004; Lacroix et al., 2013). These observations do not support the idea that the subduction seismicity would play, in the presently hyperarid conditions of the Central Western Andes, a primary role in large landslides triggering (see detailed discussion in Delgado et al., 2022).

On the other hand, the timing of the Limaxina landslide (80 ± 4 ka; Figure 5) shows some interesting correlations with terrestrial and marine paleoclimate records documented in the nearby Central Andes (Figure 6). The analysis of a sediment core from a clay pan of the Central Atacama Desert (200 km south of Limaxina), indicates

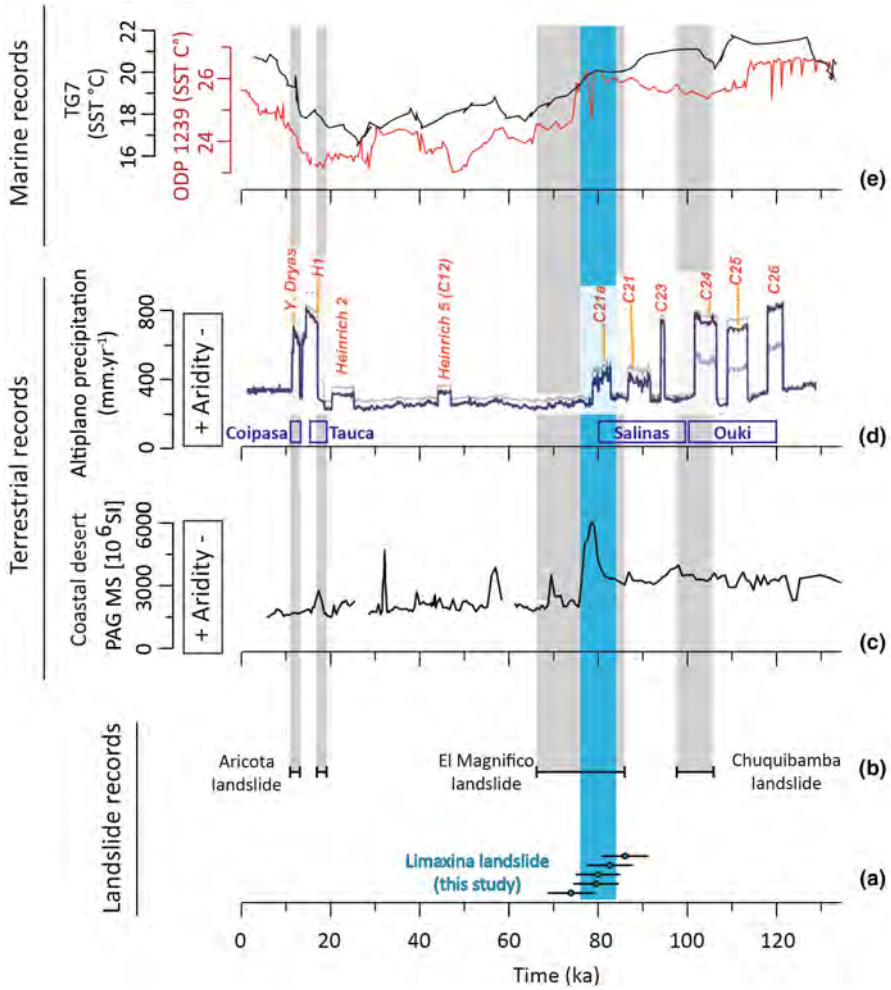

FIGURE 6 Correlation between landslides chronics, terrestrial and marine paleoenvironmental records during the late Pleistocene (see location of references on Figure 1a,b, modified and adapted from Ritter et al., 2019). (a) Timing the Limaxina landslide (in blue, this study). (b) Previously dated landslides (in grey) including the Aricota landslide (17° S) from Delgado et al. (2020), El Magnifico landslide (19° S) recalculated from Crosta et al. (2017), the Chuquibamba landslide (15° S) from Margirier et al. (2015). (c) Paleoclimate record of the hyperarid core of the Atacama Desert (21° S) from Ritter et al. (2019). (d) Altiplano paleo-precipitations (19° S) from Placzek et al. (2013) and related paleo-lake phases from Placzek et al. (2006). (e) Sea surface temperature (SST) reconstruction from East Pacific at 17°S TG7 (Calvo et al., 2001), and equatorial Pacific ODP 1239 (Rincón-Martínez et al., 2010)

that some wetter episodes have briefly interrupted the long-term hyperarid climate of the Pleistocene (Ritter et al., 2019). In particular, Ritter et al. (2019) document at ca. 80 ka a main peak of magnetic susceptibility (Figure 6c), indicating a transition from fine-grained sedimentation toward coarser grain-sizes supply. Ritter et al. (2019) related this to a significant climate change, leading to increased precipitations and fluvial activity. Ritter et al. (2019) further reported a synchronicity between these wetter events and the surface temperature of the Eastern Pacific (Figure 6e), thus resembling modern El Niño-like conditions, during which strong storms occur nowadays along the Western Andes (e.g. Bozkurt et al., 2016). Finally, the comparison with the altiplano precipitation reconstruction from Placzek et al. (2013), and its related paleolake phases, indicates also possible synchronicity with the Limaxina landslide age, correlating with the last lake high-stand of the Copaisa phase (Figure 6d). However, asynchronous climate phases between the Altiplano and the Western Andes are also subjected to discussions (e.g. Placzek et al., 2013; Ritter et al., 2019) and the uncertainties attached to our dating does not allow to differentiate between both (Figure 6). Such a persistent wet phase might have favoured high water level in the Limaxina slope, increasing the water content of the basal shales level and reducing its shear strength. Likely, it may also have increased the river discharges (here the Tarapaca Quebrada), favouring bedrock and slope toe carving which can caused the initiation of the deformation process until the slope failure occurred (excess of topography sensu Blöthe et al., 2015).

Recalculating the ^{36}Cl exposure ages of the El Magnifico rock-avalanche cluster, using up-to-date production rate and parametrization of the CREp calculator describe here above (see also Data S1 and S2), indicates a mean age of the multiple slope failures at 76 ± 10 ka which is also compatible with the previously mentioned climatic event, although the large uncertainty require caution (Figure 6b). Finally, compiling the ages of the others paleolandslides that have been dated along the Western Andes (Figure 6b), a similar scheme is revealed where paleolandslide chronics seem to correspond to wet periods. As such, even if the co-effect of seismicity on landslide triggering is probable during the time of a wet event, our findings would rather suggest a primary control of climate forcing upon seismicity. In other words, we propose that the seismicity of the Western Andes, although being very intense and permanent, is unlikely to trigger large landslide in the absence of a coeval climate forcing. This scenario would need to be further explored by dating more landslide cases. Nevertheless, if confirmed, it would suggest that the Central Western Andes could be considered as an end member case study, where it might be possible to deconvolute the effect of tectonic

and climate on landslide triggering as the region is extremely dry most of the time. At the same time, dating the landslide activities in this region would be a valuable proxy of past climate oscillations and extreme precipitations.

6 | CONCLUSION

The Limaxina paleolandslide is a large slope failure (v ~ 1 km^3) that developed at ca. 19° S and ~ 3000 m a.s.l. along the hyperarid Western Cordillera of northern Chile. Using ^{10}Be surface exposure dating, we constrained its age at 80 ± 4 ka. This timing is compatible with wet events recorded both in the Central Atacama Desert and the Altiplano lakes. The compilation of other paleo-landslide ages shows similar correspondences with the occurrence of wet periods in the Atacama Desert during the Late Pleistocene. Our results favour the view that past climate changes, rather seismicity, where the dominant forcing factor of large landslides in this hyperarid region. It calls for further dating efforts in this region hosting one the most exceptional worldwide relics of Quaternary landslides.

ACKNOWLEDGEMENTS

All the data used to perform this study are available in the paper and in the supplemental material. This work was supported by the TelluS Programs of CNRS/INSU. We acknowledge the German Aerospace Centre (DLR) for providing the TANDEM-X DEM. We gratefully thank Francis Coeur (GTC platform, Isterre Grenoble) for the sample processing. We gratefully acknowledge the ASTER Team, composed by Georges Aumaitre, Karim Keddadouche and Fawzi Zaidi, for the ^{10}Be measurements that were performed at the ASTER AMS national facility (CEREGE, Aix en Provence) which is supported by the INSU/CNRS, the ANR through the "Projets thématiques d'excellence" program for the "Equipements d'excellence" ASTER-CEREGE action and IRD. We gratefully acknowledge the Editors Salvatore Martino and Carlo Doglioni, Michele Delchiaro and one anonymous reviewer for their suggestions that improved the manuscript.

DATA AVAILABILITY STATEMENT

The data that supports the findings of this study are available in the supplementary material of this article.

REFERENCES

Armijo, R., Lacassin, R., Coudurier-Curveur, A., & Carrizo, D. (2015). Coupled tectonic evolution of Andean orogeny and global climate. *Earth-Science Reviews*, *143*, 1–35.

Arnold, M., Aumaître, G., Bourlès, D. L., Keddaddouche, K., Braucher, R., Finkel, R. C., Nottoli, E., Benedetti, L., & Merchel, S. (2013). The French accelerator mass spectrometry facility ASTER after 4 years: Status and recent developments on 36Cl and 129I. *Nuclear Instruments and Methods in Physics Research Section B: Beam Interactions with Materials and Atoms*, *294*, 24–28.

Arnold, M., Merchel, S., Bourlès, D. L., Braucher, R., Benedetti, L., Finkel, R. C., Aumaître, G., Gottdang, A., & Klein, M. (2010). The French accelerator mass spectrometry facility ASTER: Improved performance and developments. *Nuclear Instruments and Methods in Physics Research Section B: Beam Interactions with Materials and Atoms*, *268*(11–12), 1954–1959.

Binnie, A., Dunai, T. J., Binnie, S. A., Victor, P., González, G., & Bolten, A. (2016). Accelerated late quaternary uplift revealed by ^{10}Be exposure dating of marine terraces, Mejillones Peninsula, northern Chile. *Quaternary Geochronology*, *36*, 12–27.

Blöthe, J. H., Korup, O., & Schwanghart, W. (2015). Large landslides lie low: Excess topography in the Himalaya-Karakoram ranges. *Geology*, *43*(6), 523–526.

Borchers, B., Marrero, S., Balco, G., Caffee, M., Goehring, B., Lifton, N., Nishiizumi, K., Phillips, F., Schaefer, J., & Stone, J. (2016). Geological calibration of spallation production rates in the CRONUS-earth project. *Quaternary Geochronology*, *31*, 188–198.

Bozkurt, D., Rondanelli, R., Garreaud, R., & Arriagada, A. (2016). Impact of warmer eastern tropical Pacific SST on the March 2015 Atacama floods. *Monthly Weather Review*, *144*(11), 4441–4460.

Braucher, R., Bourlès, D., Merchel, S., Romani, J. V., Fernadez-Mosquera, D., Marti, K., Leanni, L., Chauvet, F., Arnold, M., Aumaître, G., & Keddadouche, K. (2013). Determination of muon attenuation lengths in depth profiles from in situ produced cosmogenic nuclides. *Nuclear Instruments and Methods in Physics Research Section B: Beam Interactions with Materials and Atoms*, *294*, 484–490.

Braucher, R., Guillou, V., Bourlès, D. L., Arnold, M., Aumaître, G., Keddadouche, K., & Nottoli, E. (2015). Preparation of ASTER in-house10Be/9Be standard solutions. *Nuclear Instruments and Methods in Physics Research Section B: Beam Interactions with Materials and Atoms*, *361*, 335–340.

Calvo, E., Pelejero, C., Herguera, J. C., Palanques, A., & Grimalt, J. O. (2001). Insolation dependence of the southeastern subtropical Pacific Sea surface temperature over the last 400 kyrs. *Geophysical Research Letters*, *28*, 2481–2484.

Candia, G., De Pascale, G. P., Montalva, G., & Ledezma, C. (2017). Geotechnical aspects of the 2015 Mw 8.3 Illapel megathrust earthquake sequence in Chile. *Earthquake Spectra*, *33*(2), 709–728.

Chlieh, M., Perfettini, H., Tavera, H., Avouac, J. P., Remy, D., Nocquet, J. M., Rolandone, F., Bondoux, F., Gabalda, G., & Bonvalot, S. (2011). Interseismic coupling and seismic potential along the Central Andes subduction zone. Journal of geophysical research: Solid. *Earth*, *116*, B12415. https://doi.org/10.1029/2010JB008166

Corbett, L. B., Bierman, P. R., & Rood, D. H. (2016). An approach for optimizing in situ cosmogenic 10Be sample preparation. *Quaternary Geochronology*, *33*, 24–34.

Cortés-Aranda, J., González, R., Fernández, V., Astudillo, L., Miller, M., Molina, D., & Oviedo, A. (2021). Neotectonic evidence for late quaternary reverse faulting in the northern Chile outer forearc (22.5° S-23° S): Implications for seismic hazard. *Journal of South American Earth Sciences*, *109*, 103219.

Crosta, G. B., Hermanns, R. L., Dehls, J., Lari, S., & Sepulveda, S. (2017). Rock avalanches clusters along the northern Chile coastal scarp. *Geomorphology*, *289*, 27–43.

Crosta, G. B., Hermanns, R. L., Frattini, P., Valbuzzi, E., & Valagussa, A. (2014). Large slope instabilities in northern Chile: Inventory, characterisation and possible triggers. In *Landslide science for a safer geoenvironment* (pp. 175-181). Springer.

Crosta, G. B., Paolo, F., Elena, V., & Hermanns, R. L. (2015). The Cerro Caquilluco–Cerrillos Negros Giant Rock Avalanches (Tacna, Peru). *IAEG – Torino*, *2014*, N159.

Delgado, F., Zerathe, S., Audin, L., Schwartz, S., Benavente, C., Carcaillet, J., Bourles, D. L., & ASTER Team. (2020). Giant landslide triggerings and paleoprecipitations in the Central Western Andes: The aricota rockslide dam (South Peru). *Geomorphology*, *350*, 106932. https://doi.org/10.1016/j.geomorph.2019.106932

Delgado, F., Zerathe, S., Schwartz, S., Mathieux, B., & Benavente, C. (2022). Inventory of large landslides along the Central Western Andes (ca. 15°–20° S): Landslide distribution patterns and insights on controlling factors. *Journal of South American Earth Sciences*, *116*, 103824.

Dunai, T. J., Gonzalez López, G. A., & Juez-Larré, J. (2005). Oligocene–Miocene age of aridity in the Atacama desert revealed by exposure dating of erosion-sensitive landforms. *Geology*, *33*(4), 321–324.

Evenstar, L. A., Mather, A. E., & Hartley, A. J. (2020). Using spatial patterns of fluvial incision to constrain continental-scale uplift in the Andes. *Global and Planetary Change*, *186*, 103119.

Evenstar, L. A., Mather, A. E., Hartley, A. J., Stuart, F. M., Sparks, R. S. J., & Cooper, F. J. (2017). Geomorphology on geologic timescales: Evolution of the late Cenozoic Pacific paleosurface in northern Chile and southern Peru. *Earth-Science Reviews*, *171*, 1–27.

Hartley, A. J., Chong, G., Houston, J., & Mather, A. E. (2005). 150 million years of climatic stability: Evidence from the Atacama Desert, northern Chile. *Journal of the Geological Society*, *162*(3), 421–424.

Herrera, C., Cassidy, J. F., Dosso, S. E., Dettmer, J., Bloch, W., Sippl, C., & Salazar, P. (2021). The crustal stress field inferred from focal mechanisms in northern Chile. *Geophysical Research Letters*, *48*(8), e2021GL092889.

Hilger, P., Gosse, J. C., & Hermanns, R. L. (2019). How significant is inheritance when dating rockslide boulders with terrestrial cosmogenic nuclide dating?—A case study of an historic event. *Landslides*, *16*(4), 729–738.

Houston, J., & Hartley, A. J. (2003). The central Andean west-slope rainshadow and its potential contribution to the origin of hyper-aridity in the Atacama Desert. *International Journal of Climatology: A Journal of the Royal Meteorological Society*, *23*(12), 1453–1464.

Junquera-Torrado, S., Moreiras, S. M., Rodriguez-Peces, M. J., & Sepulveda, S. A. (2021). Linking earthquake-triggered paleolandslides to their seismic source and to the possible seismic event that originated them in a portion of the argentine Precordillera (31°–33° S). *Natural Hazards*, *106*, 43–78. https://doi.org/10.1007/s11069-020-04447-1

Keefer, D. K., & Moseley, M. E. (2004). Southern Peru desert shattered by the great 2001 earthquake: Implications for paleoseismic and paleo-El Niño–southern oscillation records. *Proceedings of the National Academy of Sciences of the USA*, *101*(30), 10878–10883.

Lacroix, P., Zavala, B., Berthier, E., & Audin, L. (2013). Supervised method of landslide inventory using panchromatic SPOT5 images and application to the earthquake-triggered landslides of Pisco (Peru, 2007, Mw8. 0). *Remote Sensing*, *5*(6), 2590–2616.

Lifton, N., Sato, T., & Dunai, T. J. (2014). Scaling in situ cosmogenic nuclide production rates using analytical approximations to atmospheric cosmic-ray fluxes. *Earth and Planetary Science Letters*, *386*, 149–160.

Maldonado, V., Contreras, M., & Melnick, D. (2021). A comprehensive database of active and potentially-active continental faults in Chile at 1: 25,000 scale. *Scientific Data*, *8*(1), 1–13.

Margirier, A., Audin, L., Carcaillet, J., & Schwartz, S. (2015). Tectonic and climatic controls on the Chuquibamba landslide (western Andes, southern Peru). *Earth Surface Dynamics*, *2*, 1129–1153.

Martin, L. C. P., Blard, P. H., Balco, G., Lavé, J., Delunel, R., Lifton, N., & Laurent, V. (2017). The CREp program and the ICE-D production rate calibration database: A fully parameterizable and updated online tool to compute cosmic-ray exposure ages. *Quaternary Geochronology*, *38*, 25–49.

Martínez, F., Fuentes, G., Perroud, S., & Bascuñan, S. (2021). Buried thrust belt front of the western Central Andes of northern Chile: Style, age, and relationship with basement heterogeneities. *Journal of Structural Geology*, *147*, 104337.

Mather, A. E., Hartley, A. J., & Griffiths, J. S. (2014). The giant coastal landslides of northern Chile: Tectonic and climate interactions on a classic convergent plate margin. *Earth and Planetary Science Letters*, *388*, 249–256.

McPhillips, D., Bierman, P. R., & Rood, D. H. (2014). Millennial-scale record of landslides in the Andes consistent with earthquake trigger. *Nature Geoscience*, *7*(12), 925–930.

Metois, M., Vigny, C., & Socquet, A. (2016). Interseismic coupling, megathrust earthquakes and seismic swarms along the Chilean subduction zone (38–18 S). *Pure and Applied Geophysics*, *173*(5), 1431–1449.

Morandé, J., Gallardo, F., Muñoz, M., & Farías, M. (2015). Carta Guaviña, Región de Tarapacá: Servicio Nacional de Geología y Minería, Carta Geológica de Chile, Serie Geología Básica. Escala 1:100.000. Santiago.

Moreiras, S. M., & Sepúlveda, S. A. (2015). Megalandslides in the Andes of Central Chile and Argentina (32°–34° S) and potential hazards. *Geological Society, London, Special Publications*, *399*(1), 329–344.

Pánek, T., & Klimeš, J. (2016). Temporal behavior of deep-seated gravitational slope deformations: A review. *Earth-Science Reviews*, *156*, 14–38.

Pinto, L., Hérail, G., Sepúlveda, S. A., & Krop, P. (2008). A Neogene giant landslide in Tarapacá, northern Chile: A signal of instability of the westernmost Altiplano and palaeoseismicity effects. *Geomorphology*, *102*(3–4), 532–541.

Placzek, C., Quade, J., & Patchett, P. J. (2006). Geochronology and stratigraphy of late Pleistocene lake cycles on the southern Bolivian Altiplano: Implications for causes of tropical climate change. *Geological Society of America Bulletin*, *118*(5–6), 515–532.

Placzek, C. J., Matmon, A., Granger, D. E., Quade, J., & Niedermann, S. (2010). Evidence for active landscape evolution in the hyperarid Atacama from multiple terrestrial cosmogenic nuclides. *Earth and Planetary Science Letters*, *295*(1–2), 12–20.

Placzek, C. J., Quade, J., & Patchett, P. J. (2013). A 130 ka reconstruction of rainfall on the Bolivian Altiplano. *Earth and Planetary Science Letters*, *363*, 97–108.

Rech, J. A., Currie, B. S., Jordan, T. E., Riquelme, R., Lehmann, S. B., Kirk-Lawlor, N. E., & Gooley, J. T. (2019). Massive middle Miocene gypsic paleosols in the Atacama Desert and the formation of the central Andean rain-shadow. *Earth and Planetary Science Letters*, *506*, 184–194.

Rincón-Martínez, D., Lamy, F., Contreras, S., Leduc, G., Bard, E., Saukel, C., Blanz, T., Mackensen, A., & Tiedemann, R. (2010). More humid interglacials in Ecuador during the past 500 kyr linked to latitudinal shifts of the equatorial front and the intertropical convergence zone in the eastern tropical Pacific. *Paleoceanography*, *25*, PA2210.

Ritter, B., Binnie, S. A., Stuart, F. M., Wennrich, V., & Dunai, T. J. (2018). Evidence for multiple Plio-Pleistocene lake episodes in the hyperarid Atacama Desert. *Quaternary Geochronology*, *44*, 1–12.

Ritter, B., Wennrich, V., Medialdea, A., Brill, D., King, G., Schneiderwind, S., Niemann, K., Fernández-Galego, E., Diederich, J., Rolf, C., Bao, R., Melles, M., & Dunai, T. J. (2019). Climatic fluctuations in the hyperarid core of the Atacama Desert during the past 215 ka. *Scientific Reports*, *9*(1), 1–13.

Roperch, P., Gattacceca, J., Valenzuela, M., Devouard, B., Lorand, J. P., Arriagada, C., Rochette, P., Latorre, C., & Beck, P. (2017). Surface vitrification caused by natural fires in late Pleistocene wetlands of the Atacama Desert. *Earth and Planetary Science Letters*, *469*, 15–26.

Strasser, M., & Schlunegger, F. (2005). Erosional processes, topographic length-scales and geomorphic evolution in arid climatic environments: The 'Lluta collapse', northern Chile. *International Journal of Earth Sciences*, *94*(3), 433–446.

Villegas-Lanza, J. C., Chlieh, M., Cavalié, O., Tavera, H., Baby, P., Chire-Chira, J., & Nocquet, J. M. (2016). Active tectonics of Peru: Heterogeneous interseismic coupling along the Nazca megathrust, rigid motion of the Peruvian sliver, and Subandean shortening accommodation. *Journal of Geophysical Research: Solid Earth*, *121*(10), 7371–7394.

SUPPORTING INFORMATION

Additional supporting information can be found online in the Supporting Information section at the end of this article.

Appendix S1. 36Cl exposure ages from Crosta et al. (2017) recalculated with CREp.

Appendix S2. CREp template for 36Cl exposure ages recalculation from Crosta et al. (2017).

Appendix S3. CREp template for 10Be exposure ages recalculation from this study.

How to cite this article: Zerathe, S., Audin, L., Robert, X., Schwartz, S., & Carcaillet, J. (2023). Large landslide of the hyperarid Central Western Andes triggered during a humid period of the Late Pleistocene (ca. 19°S; northern Chile). *Terra Nova*, *00*, 1–11. https://doi.org/10.1111/ter.12641